# Arc Efficiency Assisted Finite Element Model for Predicting Residual Stress of TIG Welded Sheet

Kuang-Hung Tseng *
Institute of Materials Engineering, National Pingtung University of Science and Technology, Pingtung 91201, Taiwan
Email: tkh@mail.npust.edu.tw

Jie-Meng Huang
Institute of Materials Engineering, National Pingtung University of Science and Technology, Pingtung 91201, Taiwan
Email: M10045005@mail.npust.edu.tw

***Abstract*—Predicting and controlling residual stresses are critical issues in welding engineering. With advancements in computer technology, a numerical simulation technique can predict welding residual stress. To accurately simulate temperature and stress fields, the thermal cycle obtained from the finite element model must be in coincidence with an actual heat source. This study performed a Gaussian distribution of the heat flux with an effective arc radius that was selected for the finite element analysis to accurately describe the distributive nature of the heat source provided by the welding arc. The results showed that arc efficiency has an effect on temperature history during welding. The computational results of the temperature history and residual stress showed very good agreement with the corresponding experimental data. This study proposes that the simulation errors in finite element analysis can be eliminated by adjusting the Gaussian distributed spatial heat source and arc efficiency.**

***Index Terms*—TIG welding, arc efficiency, residual stress, finite element model**

## I. Introduction

During welding, a weldment is locally supplied with a moving heat source, such as an electric arc, laser beam, or electron beam that causes the temperature distribution to be inconsistent. The fusion zone (FZ) and heat-affected zone (HAZ) are typically at a temperature that is substantially higher than that of the unaffected base metal. Highly localized heat transfer and strongly non-uniform temperature fields in both the heating and cooling cycles cause non-uniform thermal expansion and contraction, resulting in inhomogeneous plastic deformation in the weld metal and surrounding areas. Consequently, tensile residual stress is permanently produced in both the FZ and HAZ that can influence the brittle fracture, fracture toughness, fatigue strength, creep strength, and stress corrosion cracking (SCC) of the weldment [1-4]. Predicting and controlling residual stress is a critical issue for welding process and fabrication engineering.

Manuscript received September 9, 2012; revised October 16, 2012; accepted October 16, 2012.
*Corresponding author at: No. 1, Hseuhfu Rd., Neipu, Pingtung 91201, Taiwan. Tel.: +886 8 7703202; Fax: +886 8 7740552.

Researchers have proposed nondestructive and locally destructive techniques to estimate the magnitude and distribution of residual stresses in welded structures. For example, Monim et al. [5] evaluated residual stress using an X-ray diffraction technique. Qozam et al. [6] evaluated residual stress using an ultrasonic wave technique. Rendler and Vigness [7], Tseng and Chou [1], and Paynter et al. [8] proposed the hole-drilling method to determine residual stress distribution in general welded structures. However, these techniques are typically limited by cost or accuracy. Therefore, it is necessary to establish additional methods for evaluating residual stress. Over the past 30 years, extensive research has been conducted using numerical and analytical procedures for calculating thermal stress during welding. Because of the complexity of the physical processes that involve transient heat transfer and plastic deformation at high temperatures, traditional mathematical solutions are inadequate. These procedures are very time consuming and, therefore, prohibitively expensive in the welding situations [9]. Because of scientific advancements in computer hardware and software, it is now possible to use a numerical simulation technique to solve nonlinear, coupled thermo-mechanical problem with a high degree of accuracy. For instance, Muraki et al. [10, 11] developed elasto-plastic finite element computer programs to calculate thermal stress and the resulting residual stress caused by a moving heat source. Kuang and Atluri [12] used a moving mesh finite element to examine a temperature field caused by a moving heat source. Teng and Lin [13] used a two-dimensional (2D) finite element model to predict the magnitude and distribution of residual stress during the one-pass arc welding process. Furthermore, three-dimensional (3D) finite element model for predicting residual stress of the weldment have been investigated by Kohandehghan et al. [14]. A finite element method plays an indispensable role in the structural integrity and quality control of welded joints.

This study performed a Gaussian distribution of the heat flux with an effective arc radius that was selected for the finite element analysis to accurately describe the distributive nature of the heat source provided by the welding arc. In this study, commercial ANSYS software performed all of the nonlinear thermo-mechanical finite


doi:10.4304/jcp.8.9.2182-2189

element simulations. The computational results for both temperature history and residual stress were compared to available experimental data to confirm the accuracy of the proposed model.

## II. Modeling Considerations

First, a moving Gaussian heat flux simulating a heat source was modeled to generate transient temperature fields in the structure at various time increments during welding. Then, temperature history outputs from thermal analysis were calculated and saved for the subsequent mechanical analysis. During the mechanical analysis, the temperature history at the nodes of the mesh was used as the thermal loadings for calculating the thermal stress and displacement fields in the structure during and after welding.

### *A. Thermal Analysis*

The transient temperature field *T(x,y,z,t)* of a structure is a function of time *t* and spatial coordinates *(x,y,z)*. The balance relation of the heat flow of a volume bounded by an arbitrary surface is given by the following equation:

$$-\left(\frac{\partial R_x}{\partial x}+\frac{\partial R_y}{\partial y}+\frac{\partial R_z}{\partial z}\right)+q=\rho\cdot C_p\frac{\partial T(x,y,z,t)}{\partial t} \tag{1}$$

where
$R_x$ : the rate of heat flow in X-direction per unit area
$R_y$ : the rate of heat flow in Y-direction per unit area
$R_z$ : the rate of heat flow in Z-direction per unit area
$q$ : internal heat generation rate
$\rho$ : density
$C_p$ : specific heat capacity
$T$ : temperature
$t$ : time

The heat transfer of a solid body in an assumed direction can be described by introducing the Fourier law in the following manner:

$$R_x=-k_x\frac{\partial T}{\partial x} \tag{2a}$$

$$R_y=-k_y\frac{\partial T}{\partial y} \tag{2b}$$

$$R_z=-k_z\frac{\partial T}{\partial z} \tag{2c}$$

where
$k_x$ : thermal conductivity coefficient in X-direction
$k_y$ : thermal conductivity coefficient in Y-direction
$k_z$ : thermal conductivity coefficient in Z-direction

Assuming that simulation model has nonlinear material properties, the parameters $k_x$, $k_y$, $k_z$, $\rho$, and $C_p$ are dependent on temperature. Combining (1) and (2) yields:

$$\frac{\partial}{\partial x}\left(k_x\frac{\partial T}{\partial x}\right)+\frac{\partial}{\partial y}\left(k_y\frac{\partial T}{\partial y}\right)+\frac{\partial}{\partial z}\left(k_z\frac{\partial T}{\partial z}\right)+q=\rho\cdot C_p\frac{\partial T}{\partial t} \tag{3}$$

Equation (3) is a differential equation that governs heat conduction in a solid body. The general solution can be obtained by accepting the initial and boundary conditions:

1. Initial conditions

The initial condition is defined as the initial temperature distribution in the material that is being welded. Assuming that there is no preheating, the initial conditions are equal to room temperature, which can be mathematically stated as:

$$T(x,y,z,0)=T_0(x,y,z) \tag{4}$$

2. Boundary conditions (Newton's law of cooling)

The specified convection surfaces acting over arbitrary surface:

$$\{q\}^T\cdot\{\eta\}=-h_f(T_B-T_s) \tag{5}$$

where
$\{q\}$ : heat flux field
$\{\eta\}$ : unit outward normal vector
$h_f$: convection heat transfer coefficient
$T_B$ : bulk temperature of the adjacent fluid
$T_s$ : temperature at the surface of the model

The positive specified heat flow is in the boundary. The heat flux to the system is input by a moving heat source on the boundary.

Combined with the boundary conditions, the governing heat conduction equation can be rewritten as the following equation:

$$[C]\cdot\left\{\dot{T}_e\right\}+[K]\cdot\{T_e\}=\{F_e\} \tag{6}$$

Let

$$[C]=\int_V\rho\cdot C_p\cdot[E]\cdot[E]^T\cdot dV$$

$$[K]=\int_V[E']^T\cdot[K]\cdot[E']\cdot dV+\int_S h_f\cdot[E]\cdot[E]^T\cdot dS$$

$$\{F_e\}=\int_V q\cdot[E]\cdot dV+\int_S h_f\cdot T_B\cdot[E]\cdot dS$$

in which

$$[E']=[L]\cdot[E]^T$$

where
$\{T_e\}$ : nodal temperature field
$[E]$ : element shape functions
$[K]$ : thermal conductivity matrix
$[L]$ : differential operator matrix

The nodal temperature field $\{T_e\}$ in the thermal model analysis can be obtained from (6). These results are then added to the mechanical model.

In this study, the material properties were assumed to be temperature dependent to obtain a high degree of

simulation accuracy [15]. The transient temperature can be computed using an extrapolation method with a two-time interval:

$$T(\tau) = T(t-\Delta t) + \frac{\tau}{\Delta t}\left[T(t-\Delta t) - T(t-2\Delta t)\right] \tag{7}$$

Let $g$ denote the temperature dependent material parameter, that is, the function of $T(\tau)$. The material parameters at time $t$ can then be expressed as the equation:

$$g = \frac{1}{\Delta t}\int_{t-\Delta t}^{t} g\left[T(\tau)\right]\cdot d\tau \tag{8}$$

*B. Mechanical Analysis*

The equilibrium equation in the mechanical analysis is considered as the following equation:

$$\sigma_{ij,j} + \rho \cdot f_i = 0 \tag{9}$$

in which

$$\sigma_{ij} = \sigma_{ji}$$

where

$\sigma_{ij}$ : stress tensor
$f_i$ : body force

According to the principle of virtual work and the divergence theorem, (9) can be rewritten in the matrix form as the following equation:

$$\int_V \{\delta\varepsilon\}^T \cdot \{\sigma\}\cdot dV = \int_S \{\delta u\}^T \cdot \{P\}\cdot dS + \int_V \rho \cdot \{\delta u\}^T \cdot \{f\}\cdot dV \tag{10}$$

and

$$\{\delta\varepsilon\} = [B]\cdot\{\delta U_e\} \tag{11a}$$

$$\{\delta u\} = [N]\cdot\{\delta U_e\} \tag{11b}$$

$$[B] = [L]\cdot[N] \tag{11c}$$

where

$\{\sigma\}$ : stress field
$\{\varepsilon\}$ : strain field
$\{u\}$ : displacement field
$\{P\}$ : surface force field
$\{f\}$ : body force field
$\{U_e\}$ : nodal displacement field
$[B]$ : strain-displacement shape functions
$[N]$ : displacement shape functions

Substituting (11) into (10) yields:

$$\int_V [B]^T \cdot\{\sigma\}\cdot dV = \{R\} \tag{12}$$

in which

$$\{R\} = \int_S [N]^T \cdot \{P\}\cdot dS + \int_V \rho\cdot[N]^T\cdot\{f\}\cdot dV \tag{13}$$

The mentioned expression is considered to denote a linear elastic model. Because the nodal displacement function is a nonlinear thermo-elasto-plastic model, this study uses an incremental calculation. For an incremental analysis, the nodal force applied to the element $\{R\}$ at step $(m+1)$ can be expressed as the following equation:

$$^{m+1}\{R\} = {}^{m}\{R\} + \{\Delta R\} \tag{14a}$$

The nodal stress $\{\sigma_e\}$ can also be described as:

$$^{m+1}\{\sigma_e\} = {}^{m}\{\sigma_e\} + \{\Delta\sigma_e\} \tag{14b}$$

Accordingly, (12) and (14) become:

$$\int_V [B]^T \cdot\{\Delta\sigma_e\}\cdot dV = {}^{m}\{R\} + \{\Delta R\} - \int_V [B]^T \cdot {}^{m}\{\sigma_e\}\cdot dV \tag{15}$$

Substituting (12) into (15) yields:

$$\int_V [B]^T \cdot\{\Delta\sigma_e\}\cdot dV = \{\Delta R\} \tag{16}$$

For the thermo-elasto-plastic material behavior, the isotropic strain-hardening rule and the von Mises yield criterion were considered. The stress and strain relations can be then defined as the following equation:

$$\{\Delta\sigma_e\} = [S^{ep}]\cdot[B]\cdot\{\Delta U_e\} - [S^{th}]\cdot[M]\cdot\{\Delta T_e\} \tag{17}$$

Let

$$[S^{ep}] = [S^{e}] + [S^{p}]$$

where

$\{\Delta\sigma_e\}$ : nodal stress increment field
$\{\Delta U_e\}$ : nodal displacement increment field
$\{\Delta T_e\}$ : nodal temperature increment field
$[S^e]$ : elastic stiffness matrix
$[S^p]$ : plastic stiffness matrix
$[S^{th}]$ : thermal stiffness matrix
$[M]$ : temperature shape functions

Substituting (17) into (16) yields:

$$^{m+1}\{K_1\}\cdot\{\Delta U_e\} - {}^{m+1}\{K_2\}\cdot\{\Delta T_e\} = \{\Delta R\} \tag{18}$$

Let

$$^{m+1}\{K_1\} = \int_V [B]^T \cdot [S^{ep}]\cdot[B]\cdot dV$$

$$^{m+1}\{K_2\} = \int_V [B]^T \cdot [S^{th}]\cdot[M]\cdot dV$$

The nodal displacement increment field $\{\Delta U_e\}$ in the mechanical analysis can be obtained from (18). With this result, the nodal stress increment field $\{\Delta\sigma_e\}$ is obtained from (17). Furthermore, the nodal stress field $\{\sigma_e\}$ can be obtained from (14b) using an iteration procedure. A full

Newton-Raphson method was used in each time step for the heat balance iteration.

## III. Analysis Methods

In the coupled thermo-mechanical analysis, a nonlinear model that included a transient computational approach was used, in which the thermophysical and mechanical properties were considered to be a function of temperature (Table I). The melting point of sheet metal was chosen to be 1400 °C. Poisson's ratio remains approximately constant at 0.3. In addition, no phase transformation occurred in the molten metal during welding.

A 3D finite element analysis of the temperature and stress fields in a welded sheet was performed using ANSYS commercial software. The thermo-mechanical finite element model included the Gaussian distributed spatial heat source, temperature dependent material properties, and coupled thermo-elasto-plastic behavior of the materials. Because of the locally concentrated heat source, the high temperature and stress gradients near the FZ changed rapidly according to the distance from the center of the heat source. A fine mesh was used on both sides of the fusion center line. This study modeled the symmetric half of the model with 6000 elements and 9792 nodes.

The heat input during welding is modeled in ANSYS by distributed heat flux applied to individual elements. In this study, heat flux is defined as the amount of heat transferred per unit area per unit time from or to a surface. Heat flux travels at a constant speed and is gradually applied to newly activated elements to generate heat energy. Furthermore, heat energy caused by welding transferred to the workpiece is determined by the arc efficiency. Arc efficiency is only slightly affected by welding parameters for a particular process [16].

## IV. Experimental Procedures

The welded sheet used in this experiment is austenitic 304 stainless steels. Sheets 3 mm in thickness were cut into strips of size 100×300 mm, which were roughly grinded with 240 grit silicon carbide abrasive paper to remove all impurities, and were subsequently cleaned with acetone prior to welding. A direct-current, electrode-negative (DCEN) power supply device was used with a mechanized operation system in which the welding torch traveled at a constant speed. Single-pass, autogenous TIG welding was performed along the centerline of the test specimen to produce a butt-joint weld. A water-cooled torch with a standard 2% thoriated tungsten electrode was used during the experiments. The electrode rod was 2.4 mm in diameter, with a 60° tip angle and an arc gap of 3 mm. Argon of 99.99% purity, at a constant flowrate of 10 l/min, was used as the shielding gas. Fig. 1 shows the TIG welding systems used in the experiments.


Figure 1. Automatic TIG welding systems.

Five K-type thermocouples were separately mounted on the sheets at distances of 2, 12, 27, 57, and 77 mm from the fusion line and transverse to the welds to record the temperature distribution during welding. Thermocouples were precalibrated by a quartz thermometer with 0.1 °C precision, and the data signals were collected and converted

TABLE I.
VARIATION OF MATERIAL PROPERTIES WITH TEMPERATURE OF THE EXPERIMENTAL SHEET METAL.

| T | 25 | 100 | 200 | 300 | 400 | 500 | 600 | 700 | 800 | 900 | 1000 | 1200 | 1400 |
|---|---|---|---|---|---|---|---|---|---|---|---|---|---|
| α | 16.9 | 17.2 | 17.5 | 17.8 | 18.1 | 18.4 | 18.7 | 18.8 | 18.9 | 19.0 | 19.1 | 19.2 | — |
| K | 14.3 | 16.4 | 18.0 | 19.4 | 20.8 | 22.3 | 23.6 | 24.6 | 25.5 | 26.3 | 27.2 | 27.5 | — |
| C | 4.70 | 5.10 | 5.35 | 5.51 | 5.64 | 5.79 | 5.95 | 6.08 | 6.20 | 6.30 | 6.38 | 6.40 | — |
| ρ | 8.02 | 7.95 | 7.90 | 7.88 | 7.85 | 7.81 | 7.75 | 7.70 | 7.65 | 7.63 | 7.61 | 7.59 | — |
| $\sigma_y$ | 295 | 223 | 187 | 166 | 152 | 141 | 132 | 124 | 110 | 85 | 55 | 10 | — |
| E | 193 | 191 | 189 | 181 | 172 | 164 | 153 | 143 | 125 | 100 | 60 | 10 | — |
| $E_T$ | 42 | 37 | 32 | 28 | 24 | 20 | 16 | 13 | 10 | 8 | 6 | 4 | — |

T, temperature: °C
α, thermal expansion: $10^{-6}$ m/m °C
K, thermal conductivity: W/m °C
C, specific heat: $10^2$ J/Kg °C
ρ, density: $10^3$ Kg/m$^3$
$\sigma_y$, yield stress: $10^6$ Pa
E, elasticity modulus: $10^9$ Pa
$E_T$, tangent modulus: $10^8$ Pa

by a data acquisition system. After welding, the three-element strain gage rosettes were attached at certain locations on the weldment surface. Using a high-speed drilling machine, a hole with a diameter of 1.6 mm was drilled in the center of the rosette to measure the residual stress of the weldment. The welding residual stress was determined using the hole-drilling strain-gage method given in ASTM standard E837.

## V. Results And Discussion

### A. Arc Efficiency

Pavelic et al. [17] proposed the concept of a distributed heat source with a Gaussian function $q(r)$ to represent a welding arc that can be expressed by the equation:

$$q(r) = q_m \exp(-Cr^2) \tag{19}$$

where $q_m$ is the maximum heat flux, $C$ is an adjustable constant, and $r$ is the distance from the arc center.

The power input of the heat source (arc power) $Q$ describes the heat flux of the arc. $Q$ equals $\eta IV$, where $\eta$ is arc efficiency, $I$ is welding current, and $V$ is arc voltage. The heat flux from the arc can be expressed by the equation:

$$q(r) = \frac{3Q}{\pi a^2} \exp(-\frac{3r^2}{a^2}) \tag{20}$$

where $a$ is the characteristic parameter of arc distribution, which can be considered the value of the arc radius.

Note that the arc radius was determined from experimental work and was expressed as a main function of the welding current, travel speed, arc length, and electrode geometry in the TIG welding.

For accurate simulation of the temperature and stresses, the temperature history obtained from the finite element model was the actual heat source. A Gaussian function with an effective arc radius was chosen for use in the finite element analysis to more accurately describe the distributive nature of the heat source provided by the welding arc. To calculate the distribution and magnitude of the heat source, the value of the effective arc radius must be determined through a dimension of the actual arc column. Therefore, a charge-coupled device detector system was used to observe and record the images of the welding arc profile. Fig. 2 shows a clear arc profile of the actual TIG welding for a current of 110 A and an arc length of 3 mm. This figure shows that the effective arc radius is 2.7 mm.

To investigate the effect of arc efficiency on the thermal cycle of the weldment, five values of arc efficiency were considered. In this study, the arc power was assumed to be 701.8, 765.6, 829.4, 893.2, and 957.0 W, corresponding to the following TIG welding parameters: a current of 110 A, a voltage of 11.6 V, and the arc efficiency of 0.55, 0.60, 0.65, 0.70, and 0.75, respectively. The travel speed of a Gaussian heat flux with an effective arc radius of 2.7 mm was assumed as 5 mm/sec, yielding a 60 s total welding time. Fig. 3 shows the peak temperature distribution in the TIG weldment produced with various arc efficiencies. The arc efficiency affected the temperature distributions during welding. As arc efficiency increased, the peak temperature of the TIG weldment increased. Because the calculated arc power was proportional to the arc efficiency, increased arc efficiency had the positive effect of increasing the quantity of energy generated by the arc per unit length of the welds. In fact, changing the arc efficiency was equivalent to changing the effective heat generation rate. Compared to the experimental results, the finite element model results for arc efficiency of 0.65 agreed well with the measured data, as shown in Fig. 4.

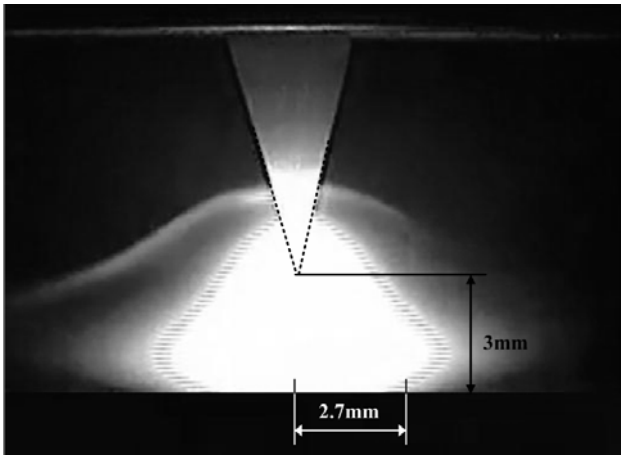


Figure 2. Arc profile of actual TIG welding.

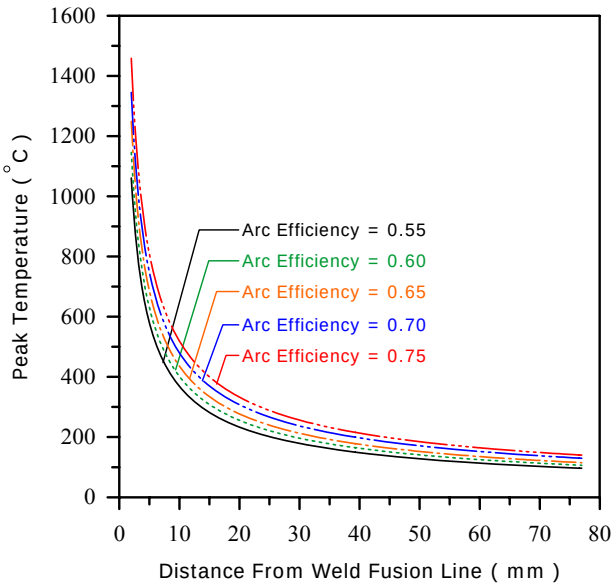


Figure 3. Distribution of peak temperature of weldment produced with various arc efficiencies.

### B. Temperature History

Computational simulation was performed under the same TIG welding parameters: the welding current was 110 A, arc voltage was 11.6 V, and travel speed was 5 mm/sec. A Gaussian heat flux with an effective arc radius of 2.7 mm and an arc efficiency of 0.65 were used to perform all of the thermo-mechanical analyses for the heat flux applied to the welded sheet.

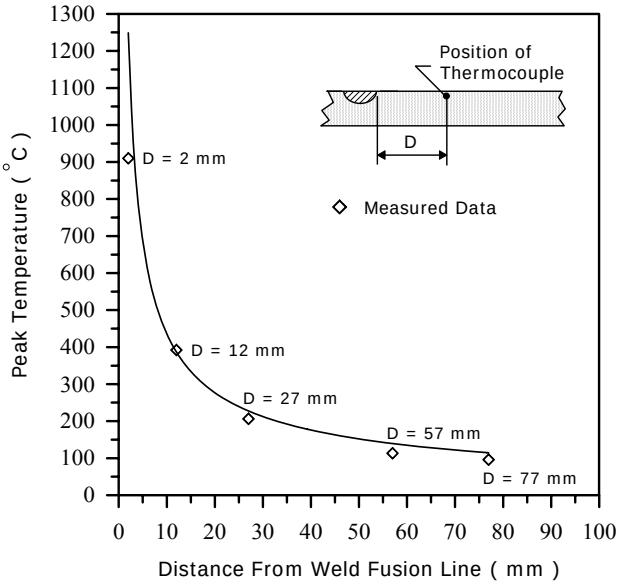


Figure 4. Peak temperature of weldment comparison between computational and experimental results for arc efficiency of 0.65.

Fig. 5 shows the temperature history during the heating and cooling cycles, which was observed computationally and experimentally. A comparison of the simulated results and measured data clearly indicated that this thermal model offers a good estimation of temperature distributions reached at certain locations of the welded sheet.

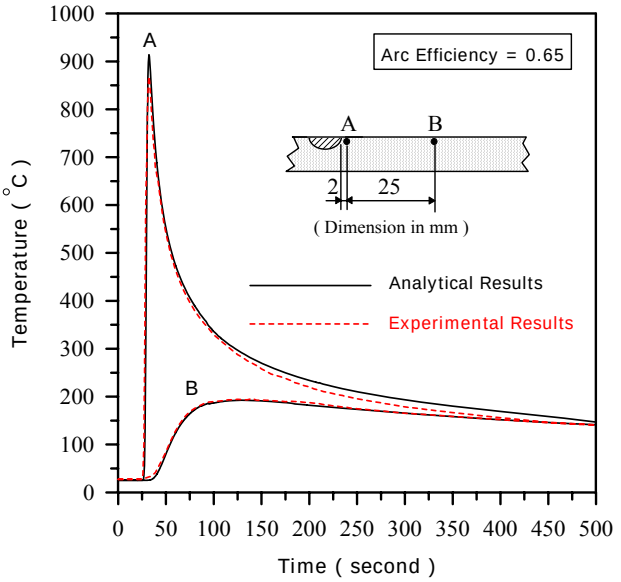


Figure 5. Temperature history during heating and cooling cycles.

## C. Thermal Stress

A thermal stress analysis was required to estimate the magnitude and distribution of the residual stresses that varied over time.

Fig. 6 shows the distribution of longitudinal thermal stress ($\sigma_{l\text{-}th}$) as the heat source reached the middle of the weldment. The action of $\sigma_{l\text{-}th}$ along the Y-direction can be described as follows:

1. Along Line A (which precedes the heat source)

Because the heat source was away from Line A, the $\sigma_{l\text{-}th}$ caused by welding was nearly zero.

2. Along Line B (which crosses the heat source)

Along Line B, the $\sigma_{l\text{-}th}$ was close to zero in the region underneath the heat source because the molten pool could not support the thermal load. The molten pool was in a zero stress state. In the regions further away from the heat source, the $\sigma_{l\text{-}th}$ was in a compressive state because the expansion of these regions was restrained by the surrounding cold metal. However, the $\sigma_{l\text{-}th}$ in regions far away from the heat source were in a tensile state and had to be balanced with compressive $\sigma_{l\text{-}th}$ in regions near the heat source for mechanics-equilibrium reasons.

3. Along Line C (which follows the heat source)

Along Line C, the FZ cooled and had a tendency to contract. This produced a higher tensile $\sigma_{l\text{-}th}$ in the regions close to the FZ. As the distance from the FZ increased, the $\sigma_{l\text{-}th}$ first changed to a compressive state, but then became tensile.

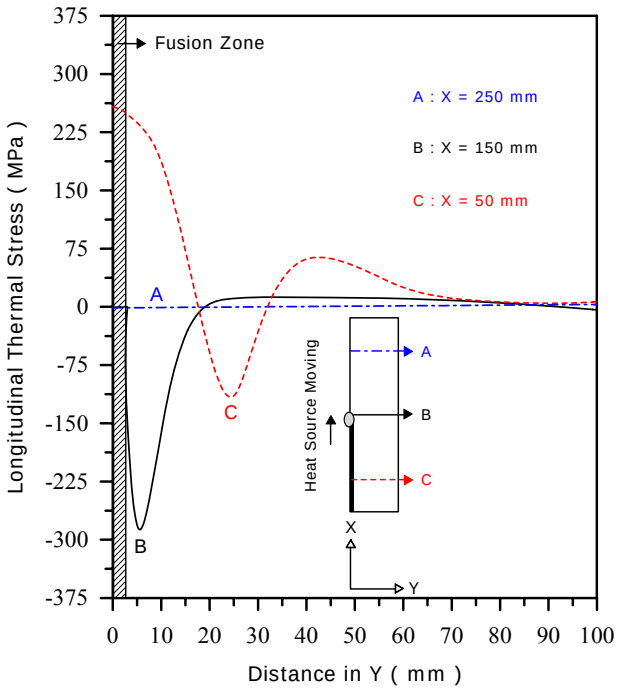


Figure 6. Distribution of longitudinal thermal stresses.

Fig. 7 shows the distribution of transverse thermal stress ($\sigma_{t\text{-}th}$) as the heat source reached the middle of the weldment. The action of $\sigma_{t\text{-}th}$ along the X-direction can be considered as follows:

1. Along Line D (close to the heat source)

Because the temperature changed rapidly with the initial heat-up, regions closest to the heat source can produce a substantial amount of compressive $\sigma_{t\text{-}th}$. Tensile $\sigma_{t\text{-}th}$ is induced to equilibrium with the compressive $\sigma_{t\text{-}th}$ in the regions farther away from the heat source. A large compressive $\sigma_{t\text{-}th}$ appeared just ahead of the heat source along Line D.

2. Along Line E (away from the heat source)

Because Line E is farther away from the heat source, the distribution of $\sigma_{t\text{-}th}$ did not clearly change along Line E.

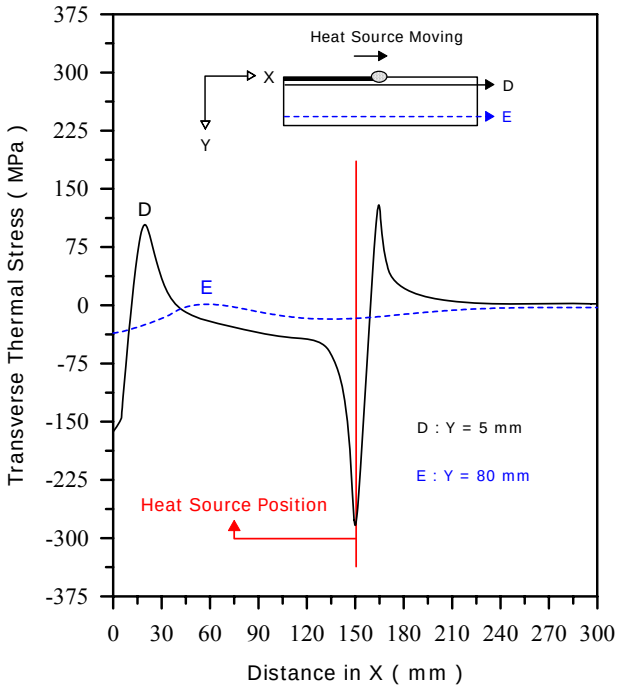


Figure 7. Distribution of transverse thermal stresses.

### *D. Residual Stress*

To obtain the same initial stress state before welding, the test specimens were annealed at a temperature of 900 °C for 2 h. The initial stresses of the test specimens were measured using the hole-drilling strain-gage method to evaluate the residual stresses induced after welding. The test specimens had an average principal stress of 6.2 MPa that was 2.1% of the yield stress of the specimen that was used. Because the value was small, the initial stress was neglected in this study.

Fig. 8 shows the distribution of longitudinal residual stress ($\sigma_{l\text{-}re}$) in the weldment cool-down at room temperature. As the heat source passed by, the FZ cooled and had a tendency to contract. A substantial tensile $\sigma_{l\text{-}re}$ was produced in the FZ, but this stress rapidly decreased to zero over a distance that was several times greater than the FZ. Farther away from the FZ, it became a compressive $\sigma_{l\text{-}re}$ for self-equilibrating purposes. Furthermore, the middle of the weldment (X: 150 mm and Y: 0 mm) exhibited a maximum tensile $\sigma_{l\text{-}re}$ (about 293 MPa) at magnitudes similar to the yield stress of the test specimen. This is because restrained thermal expansion and contraction in the middle of the weldment were present in large amounts. An approximately 46 mm tensile residual stress zone (TRSZ) was found in the weldment with the current of 110 A, voltage of 11.6 V, and travel speed of 5 mm/sec. The heat input per unit length of a weld was the most significant factor affecting the range of TRSZ [1], which had an increasing amount of heat input. The TRSZ can significantly influence mechanical and corrosion properties (such as fracture toughness, fatigue strength, and SCC) in welded structure.

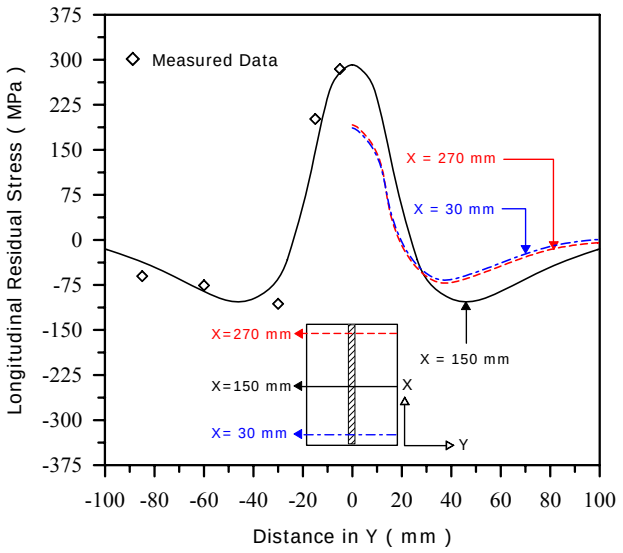


Figure 8. Distribution of longitudinal residual stresses.

Fig. 9 shows the distribution of transverse residual stress ($\sigma_{t\text{-}re}$) in the weldment cool-down at room temperature. Along Line A, the maximum tensile $\sigma_{t\text{-}re}$ occurred in regions farther away from the middle of the weldment. The maximum tensile $\sigma_{t\text{-}re}$ (about 95 MPa) was only one-third of the maximum tensile $\sigma_{l\text{-}re}$, and the compressive $\sigma_{t\text{-}re}$ could be induced at the start and end of the weldment. The maximum compressive $\sigma_{t\text{-}re}$ (about 285 MPa) was greater than the maximum tensile $\sigma_{t\text{-}re}$. Furthermore, the magnitudes of maximum tensile and compressive $\sigma_{t\text{-}re}$ decreased as the distance from the FZ increased. At a greater distance (across Line C), the maximum $\sigma_{t\text{-}re}$ changed from compressive to tensile conditions at the start and end of the weldment.

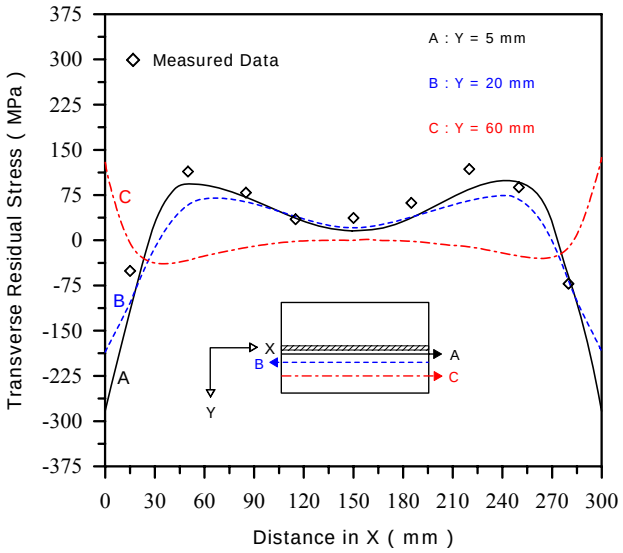


Figure 9. Distribution of transverse residual stresses.

The experimentally measured residual stress values obtained from the hole-drilling strain-gage method were plotted and are shown in Figs. 8 and 9. As a whole, the measured data at certain locations of the weldments, compared to the computational predictions, matched well with the experimental results.

## VI. Conclusions

This study created a nonlinear finite element model associated with arc efficiency to simulate the temperature distributions during welding and the residual stresses of the welded sheet. Analysis model included the Gaussian distributed spatial heat source, temperature dependent material properties, and coupled thermo-elasto-plastic behavior of the materials. The results showed that arc efficiency has an affect on the temperature history during welding. Comparison between the computational results and experimental data indicated good agreement. The greatest value of this study does not lie in its ability to predict the magnitude and distribution of the temperature history and residual stress of the weldment, but rather, this study proposes that simulation errors in finite element analysis that can be eliminated by adjusting the Gaussian distributed spatial heat source and arc efficiency.

## Acknowledgment

The authors gratefully acknowledge the financial support provided to this study by the National Science Council, Taiwan under the grant no. 100–2622–E–020–006–CC3.

## References

[1] K. H. Tseng, C. P. Chou, "The effect of pulsed GTA welding on the residual stress of a stainless steel weldment," *Journal of Materials Processing Technology*, vol. 123, pp. 346–353, 2002.
[2] D. Deng, "FEM prediction of welding residual stress and distortion in carbon steel considering phase transformation effects," *Materials and Design*, vol. 30, pp. 359–366, 2009.
[3] I. Weich, T. Ummenhofer, "Effects of high-frequency peening methods on the surface layers and the fatigue strength of welded details," *Materials and Manufacturing Processes*, vol. 26, pp. 288–293, 2011.
[4] C. Acevedo, A. Nussbaumer, "Effect of tensile residual stresses on fatigue crack growth and S–N curves in tubular joints loaded in compression," *International Journal of Fatigue*, vol. 36, no. 1, pp. 171–180, 2012.
[5] V. I. Monin, T. Gurova, X. Castello, S. F. Estefen, "Analysis of residual stress state in welded steel plates by X-ray diffraction method," *Reviews on Advanced Materials Science*, vol. 19, pp. 172–175, 2009.
[6] H. Qozam, S. Chaki, G. Bourse, C. Robin, H. Walaszek, P. Bouteille, "Microstructure effect on the lcr elastic wave for welding residual stress measurement," *Experimental Mechanics*, vol. 50, no. 2, pp. 179–185, 2010.
[7] N. J. Rendler, I. Vigness, "Hole-drilling strain-gauge method of measuring residual stresses," *Experimental Mechanics*, vol. 6, no. 12, pp. 577–586, 1066.
[8] R. Paynter, A. H. Mahmoudi, M. J. Pavier, D. A. Hills, D. Nowell, C. E. Truman, D. J. Smith, "Residual stress measurement by deep hole drilling and trepanning-analysis with distributed dislocations," *Journal of Strain Analysis*, vol. 44, no. 1, pp. 45–54, 2009.
[9] M. Adak, N. R. Mandal, "Numerical and experimental study of mitigation of welding distortion," *Applied Mathematical Modelling*, vol. 34, pp. 146–158, 2010.
[10] T. Muraki, J. J. Bryan, K. Masubuchi, "Analysis of thermal stresses and metal movement during welding part I: analytical study," *Journal of Engineering Materials and Technology*, vol. 97, no. 1, pp. 81–84, 1975.
[11] T. Muraki, J. J. Bryan, K. Masubuchi, "Analysis of thermal stresses and metal movement during welding part II: comparison of experimental data and analytical results," *Journal of Engineering Materials and Technology*, vol. 97, no. 1, pp. 85–91, 1975.
[12] Z. B. Kuang, S. N. Atluri, "Temperature field due to a moving heat source: a moving mesh finite element analysis," *Journal of Applied Mechanics*, vol. 52, pp. 274–280, 1985.
[13] T. L. Teng, C. C. Lin, "Effect of welding conditions on residual stresses due to butt welds," *International Journal of Pressure Vessels and Piping*, vol. 75, pp. 857–864, 1998.
[14] A. R. Kohandehghan, S. Serajzadeh, A. H. Kokabi, "A study on residual stresses in gas tungsten arc welding of AA5251," *Materials and Manufacturing Processes*, vol. 25, pp. 1242–1250, 2010.
[15] Y. C. Chen, K. H. Tseng, Y. S. Cheng, "Electrode displacement and dynamic resistance during small-scale resistance spot welding," *Advanced Science Letters*, vol. 11, pp. 72–79, 2012.
[16] J. N. DuPont, A. R. Marder, "Thermal efficiency of arc welding processes," *Welding Journal*, vol. 74, no. 12, pp. 406–416, 1995.
[17] V. Pavelic, R. Tanbakuchi, O. A. Uyehara, P. S. Myers, "Experimental and computed temperature histories in gas tungsten arc welding of thin plates," *Welding Journal*, vol. 48, no. 7, pp. 295–305, 1969.

**Kuang-Hung Tseng** (1973) received his PhD degree in Department of Mechanical Engineering, National Chiao Tung University, Taiwan in 2001. He is currently an associate professor at the Institute of Materials Engineering, National Pingtung University of Science and Technology, Taiwan. His research fields include advanced joining processes, mechanical properties testing, materials failure analysis, and metal corrosion & protection.

**Jie-Meng Huang** (1980) received his BS degree in Department of Business Administration, Ming Chuan University, Taiwan in 2004. He is currently a master student at the Institute of Materials Engineering, National Pingtung University of Science and Technology, Taiwan. He is also a senior engineer in Wel & Cut Co. Ltd. His research interests include materials welding technology, operation & maintenance of arc welding machine.